physica status solidi (a)

RESEARCH ARTICLE

Hybrid Oligomeric Metal Complex: A Dual Electron Transport Medium for Organic Light-Emitting Diodes

Basil A. Abdullah[1] | Raed K. Zaidan[2] | Hanan A. Al-Hazam[2] | Hameed A. Al-Attar[1]

[1]Physics Department, College of Science, University of Basrah, Basrah, Iraq | [2]Chemistry Department, College of Science, University of Basrah, Basrah, Iraq

Correspondence: Basil A. Abdullah (basil.abdullah@uobasrah.edu.iq)

Received: 27 October 2025 | **Revised:** 28 November 2025 | **Accepted:** 2 December 2025

Keywords: 1,3,4-oxadiazole | 8-hydroxyquinoline | electron-transport material | oligomeric metal complex | organic light-emitting diode | time-resolved analysis

ABSTRACT

A new hybrid monomer ligand, termed B8HQOXD **5**, is successfully synthesized. This ligand is composed of 5,5′-((((1,3,4-oxadiazole-2,5-diyl)bis(1,4-phenylene))bis(azanediyl))bis(methylene))bis(quinolin-8-ol). The corresponding oligomer metal complex, B8HQOXD–Zn(II) **6**, is also designed and synthesized. Through meticulous spectroscopic analyses, we have explored the luminescent behavior of our oligomer **6** as a function of temperature and time. This exploration has revealed three distinct luminance emissions, each mirroring a distinct structural aspect of oligomer **6**. These emissions have been meticulously correlated with various origin groups, offering a comprehensive understanding of the oligomeric structure. When compound **6** is utilized at low concentrations, it demonstrates promising electron-transport properties in solution-processed organic light-emitting diodes with a specific device structure: glass/indium tin oxide/PEDOT:PSS/PVK + 10% [**6**] + 4% $Ir(ppy)_3$/LiF/Al.

1 | Introduction

Organic light-emitting diodes (OLEDs) have garnered considerable interest for their potential as flat-panel displays [1] and efficient lighting sources [2]. The efficiency of OLED devices hinges upon several crucial physical parameters, encompassing electrode design, active layer thickness and structure, doping concentration and type, as well as carrier transport and balance [3]. Understanding the intricate processes of carrier injection, transportation, and exciton formation within mixed systems is paramount in optimizing OLED performance [4]. To achieve efficient OLEDs with a single-layer configuration, the organic emitting layer (EL) material should possess high luminescence yield and enable efficient injection and transport of both electrons and holes. Most highly fluorescent or phosphorescent organic materials suitable for OLEDs tend to function as either hole-transport (p-type) or electron-transport (n-type) components. This necessitates the incorporation of additional materials—either electron injection/transport (EIT) or hole injection/transport (HIT) materials—to establish a balanced electron–hole injection and transport environment. Although, bipolar (donor–acceptor), thermally activated delayed fluorescence materials have demonstrated potential in fulfilling both hole and electron-transport functions in the emissive layer [5]. Nevertheless, additional layers are still required for electron injection and hole blockage to confine the generated excitons in the emissive layer [6]. In single-layer configuration solution-processable OLED devices with a p-type host material, the EIT material must be mixed with the host material in a relatively high concentration (40%–50% ww) to achieve a suitable balance with hole transport [7]. The utilization of oxadiazoles, notably the molecule 2-(4-biphenyl)-5-(4-tert-butylphenyl)-1,3,4-oxadiazole (PBD), has been widespread as electron-transport materials [8–13]. However, the crystallization of vacuum-evaporated PBD thin films due to joule heating during device operation leads to decreased device longevity. To address the need for efficient EIT materials at lower concentrations, particularly for single-layer solution-processable OLEDs, researchers have proposed oligomeric oxadiazole as a promising alternative [14]. Furthermore, metal chelates based on substituted 8-hydroxyquinoline (8-HQ) and Group II metal ions, such as Be(II) and Zn(II), have also found applications in OLEDs. Notably, 8-hydroxyquinoline chelates, exemplified by tris(8-hydroxyquinolinato) aluminum (8HQ-Al) have played a seminal role in early organic light-emitting devices

due to their favorable properties, including high fluorescence, thermal stability, and excellent electron-transport mobility [15, 16]. These metal–quinoline complexes continue to be of great interest as high-performance light-emitting materials [17, 18]. Despite previous attempts at synthesizing oligomeric metal complexes containing 8-hydroxyquinoline in the oligomer backbone [19, 20], none have explored the integration of the 1,3,4-oxadiazole motif and 8-hydroxyquinoline in a single compound.

In this study, a new electron-transport material has been successfully synthesized by combining two distinct monomers (hybrid monomer), resulting in B8HQOXD **5** and the corresponding oligomeric metal complex B8HQOXD–Zn(II) **6**. The photophysical properties of the synthesized materials have been extensively characterized using UV–vis absorption and fluorescence emission spectrum analysis in a diluting solution. Additionally, time-resolved analysis of the oligomeric metal complex **6** in a PMMA film was conducted, yielding valuable insights into the material's spectral emissions. Of particular note is the successful application of compound **6**, used at low concentration, as an electron-transport material in solution-processed OLED devices. The specific device structure employed was glass/indium tin oxide (ITO)/PVK (40 mg/ml) + 10% [**6**] + 4% $Ir(ppy)_3$/LiF(1 nm)/Al(100 nm). Moreover, the demonstrated bioactive potential of both electron-transport groups in this oligomeric structure against various bio targets, including microorganisms, tumor cells, and receptors [21], further highlights the compound's versatility and potential applications in the realm of bioactive oligomers.

2 | Experimental Section

2.1 | Materials and Methods

P-Aminobenzoic acid, hydrazine hydrate, phosphorus pentoxide, ortho-phosphoric acid, zinc chloride, sodium methoxide, potassium hydroxide, 8-hydroxy quinoline, formalin, hydrochloric acid, *N, N*-dimethylformamide (DMF), dimethyl sulfoxide (DMSO), ethyl, and methyl alcohol were procured from reputable suppliers such as Aldrich, Merck, and Fluka. For material analysis, an FTIR spectrum was recorded using a Shimadzu spectrophotometer with KBr pellets as the sample holder. 1H NMR spectra were recorded on a Bruker NMR 400 spectrometer operating at 400 MHz and at room temperature in DMSO-d_6. Tetramethylsilane (TMS) served as the internal reference. Molecular weight determination was carried out using gel permeation chromatography (GPC) methodology.

2.2 | Photophysical Instrumentation

UV–vis spectra and photoluminescence (PL) spectra were acquired for all samples using a Shimadzu UV-3600 spectrometer (spectrometer range 185–3300 nm) and a Jobin Yvon (FluoroMax-3) luminescence spectrometer (Xenon arc-lamp excitation), respectively. Time-resolved spectra were obtained by exciting the samples with a pulsed YAG laser operating at 150 ps, 10 Hz, and 355 nm ND. The emission was directed at a spectrograph and synchronized ICCD (Stanford Computer Optics) camera. For obtaining PL decay transients, time delay steps and integration times were systematically increased, following the procedure described in the Supporting Information.

2.3 | OLED Devices Preparation

OLED devices were fabricated on ITO-coated glass substrates with a thickness of 125 nm and a sheet resistance of 20 Ω/□. A poly(3,4-ethylenedioxy-thiophene) doped with a high work function hole-injection layer (HIL) poly(styrenesulfonic acid) (PEDOT:PSS) was spin-coated at 2500 rpm for 60 s to form a 60 nm thick HIL. These HIL-coated substrates were annealed at 200°C for 5 min on a hot plate to remove residual water. The oligomeric complex B8HQOXD–Zn(II) exhibits excellent solubility in DMSO; however, DMSO cannot be used to form high-quality thin films for OLED devices. This limitation arises because DMSO is a nonvolatile solvent and other components in the device structure, such as PVK, are not soluble in DMSO. Therefore, a suitable volatile solvent was required for OLED device fabrication. To identify an appropriate solvent, we examined the solubility and PL behavior of B8HQOXD–Zn(II) in various solvents, including chlorobenzene, toluene, and anhydrous benzonitrile. The PL spectra (Figure S5) clearly show that incomplete dissolution leads to aggregation, evident from the appearance of a red-shifted excimer emission and a broader, less structured PL profile. Among the solvents tested, chlorobenzene provided the best solubility and stable PL emission, confirming it as the most suitable volatile solvent for OLED device preparation. A solution of poly(9-vinylcarbazole) (PVK) with a concentration of 30 mg/mL in chlorobenzene, acting as the high triplet host oligomer and hole-transport material, was employed. The PVK solution was doped with varying weight percentages (5%, 10%, 15%, 20%, 30%, and 40% w/w) of the electron-transport oligomer **6** to achieve charge-carrier balance. Additionally, the PVK: **6**, solution was further mixed with 4% w/w of the Ir complex fac-$Ir(ppy)_3$ to form blended devices. The prepared mixtures were filtered with a 0.45 μm pore filter and dynamically spin-coated at 2500 rpm for 1 min on top of the PEDOT:PSS layer, after which they were baked for 10 min at 120°C. Each sample was shadow masked to produce four identical devices of area 4 × 5 mm; the samples were then introduced into a nitrogen glove box, where 1 nm LiF interlayer were evaporated onto the device at a rate of 0.1 Å s−1 under vacuum at a pressure of ca. 1 × 10−6 Torr. This was followed by the deposit of a 100 nm aluminum cathode layer under the same evaporative conditions. All samples were encapsulated inside the glove box using a DELO UV-cured epoxy (KATIOBOND), capped with a 1.2 × 1.2 cm microscope glass slide, and then they were exposed to UV light for 3 min.

The current–voltage (*I–V*) characteristics and emission intensities were measured in a calibrated integrating sphere. Data acquisition was managed through a custom NI LabView program, which controlled an Agilent Technologies 6632B power supply. Electroluminescence (EL) spectra were recorded using an Ocean Optics USB 4000 CCD spectrometer, coupled with a 400 μm fiber optic.

2.4 | Monomers Synthesis

2.4.1 | Synthesis of 2,5-Bis(p-aminophenyl)-1,3,4-oxadiazole 2

2,5-Bis(p-aminophenyl)-1,3,4-oxadiazole **2** was prepared by treating para-aminobenzoic acid **1** with a mixture of hydrazine hydrate and polyphosphoric acid (PPA), following a previously reported

method. The resulting compound exhibited a melting point (Mp) of 259–261°C and was obtained with a yield of 86% [22].

2.4.2 | Synthesis of 5-Chloromethyl-8-hydroxyquinoline hydrochloride 4

5-Chloromethyl-8-hydroxyquinoline hydrochloride (**4**) was synthesized according to a previously reported procedure [23]. A mixture of 8-hydroxyquinoline 3 (7.3 g, 50 mmol), concentrated hydrochloric acid (10 mL), and 37% formaldehyde (8 mL, 50 mmol) was treated with gaseous hydrogen chloride for 90 min. The resulting yellow solid was collected via filtration and dried to yield 8.9 g (77.5% yield), with a Mp of 281°C.

2.4.3 | Synthesis of 5,5′-((((1,3,4-oxadiazole-2,5-diyl) bis(1,4-phenylene))bis(azanediyl))bis(methylene)) bis(quinolin-8-ol) (B8HQOXD) 5

A mixture of 2,5-bis(p-aminophenyl)-1,3,4-oxadiazole **2** (2.52 g, 10 mmol), CH_3ONa (0.54 g, 10 mmol), DMSO (15 ml), and KOH (0.56 g, 10 mmol) was stirred at room temperature for 2 h. Subsequently, 5-chloromethyl-8-hydroxyquinoline **4** (4.6 g, 24.3 mmol) dissolved in DMSO (20 ml) was slowly added to the above solution. The mixture was further stirred at room temperature for 10 h and then heated to 70°C for an additional 2 h. After adding water (100 ml) and neutralizing the reaction solution with a 10% hydrochloric acid solution, the precipitate was recrystallized by dissolved in ethanol and the ethanol solution was added to ice water (50 ml) to yield the purified product **5**. The yield for this synthesis was 51%. See Supporting Information for further details.

2.5 | Oligomer Synthesis

2.5.1 | Synthesis of Oligomeric Complex B8HQOXD–Zn(II) 6

The oligomeric complex B8HQOXD–Zn(II) **6** was synthesized and purified as shown in Scheme 1. A methanol solution (10 mL) of $ZnCl_2$ (0.817 g, 6 mmol) was added to a DMF solution (25 mL) of B8HQOXD **5** (2.40 g, 4 mmol). The resulting reagent mixture was stirred for 24 h at 80°C. Subsequently, the reaction mixture was subjected to filtration, and the obtained precipitate was washed with absolute methanol and dried in a vacuum oven at 50°C, resulting in the formation of a pale yellow solid. The yield of the synthesized oligomeric complex was 2.33 g, representing 87% of the expected product.

The new ligand underwent comprehensive characterization using 1H NMR spectroscopy (see Figure S1). On the other hand, characterization of the new oligomeric metal complex was solely achieved through FTIR analysis, as the complex exhibited poor solubility in most common solvents. Additionally, the molecular weight of the oligomeric metal complex was determined using GPC, analysis was carried out on waters 515–2410 system using polystyrene standards as molecular weight references and DMSO containing 0.1 M LiBr as eluent.

3 | Results and Discussion

3.1 | Synthesis Method and Characterization

The synthesis routes for all compounds are depicted in Scheme 1. 5-(Chloromethyl)-8-hydroxyquinoline hydrochloride

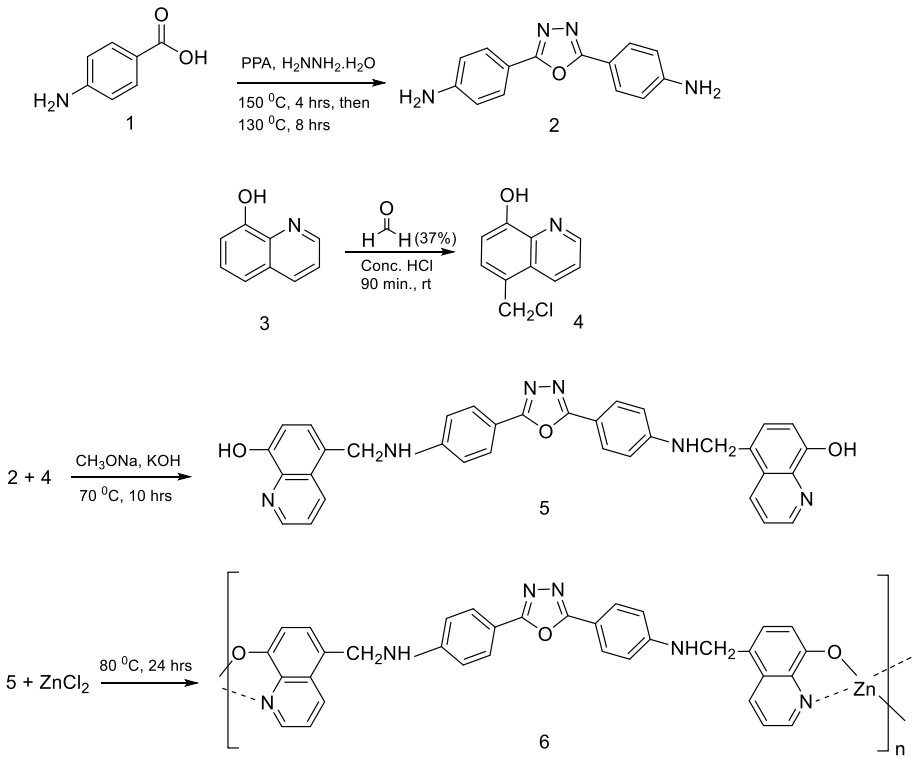

SCHEME 1 | Synthesis of oligomeric complexes B8HQOXD–Zn(II) **6**.

was successfully synthesized through the chloromethylation of 8-hydroxyquinoline using paraformaldehyde and hydrochloric acid. Subsequently, the ligand B8HQOXD **5** was synthesized by means of a condensation reaction involving 2,5-bis(p-aminophenyl)-1,3,4-oxadiazole **2** and 5-(chloromethyl)-8-hydroxyquinoline chloride **4**. To form the oligomeric metal complexes, ligand **5** was reacted with $ZnCl_2$ in a stoichiometric ratio. The new ligand exhibited excellent solubility in DMSO but showed limited solubility in several other commonly used organic solvents. Likewise, the oligomeric metal complex was highly soluble in DMSO while displaying reduced solubility in most standard organic media. It is worth noting, however, that the oligomer demonstrates good solubility in volatile aromatic solvents such as chlorobenzene. This is particularly important for OLED fabrication, where solvents like chlorobenzene are required to produce uniform and high-quality thin films, as discussed in the device preparation section. Notably, the oligomerization process was conducted under mild conditions. The FTIR spectra of the newly synthesized oligomeric complex **6** are depicted in Figure S2, further corroborating the successful synthesis of both the ligand and the oligomeric metal complex. The molecular weight analysis revealed the formation of four replicate units in the oligomer, attesting to its oligomeric nature. Overall, these results provide strong evidence of the successful synthesis of the ligand and the associated metal complex.

3.2 | Chemical Properties

The 1H NMR spectrum of B8HQOXD **5**, recorded in DMSO-d_6 solvent, is presented in Figure S1. The distinct proton signals observed at δ 9.75, 8.91, 8.50, 7.75, 7.6, 7.50, 7.10, 6.90, 6.75, and 4.65 ppm can be readily assigned to their respective protons, indicating the presence of the hydroxyquinoline and oxadiazole motifs. Specifically, the proton signal at δ 9.75 ppm corresponds to the H–O proton of the quinoline, while the signal at δ 4.65 ppm corresponds to the aliphatic CH_2. The peak at 2.5 ppm assigned to the solvent DMSO-d_6 and the peak at 3.33 ppm normally assigned to the water content in the DMSO-d_6.

Characterization of the new oligomeric metal complex was conducted through FTIR analysis. The FTIR spectra of the oligomeric complex (Figure S2) revealed several notable absorption signals. An absorption signal at 3386 cm^{-1} indicated the presence of a NH band stretching frequency. The absorption signals at 3100 cm^{-1} were attributed to the ═CH stretching frequency of the benzene ring. Additionally, the new complex exhibited C═N and C═C band stretching frequencies at 1660 and 1608 cm^{-1}, respectively. Furthermore, new sharp bands at 520 cm^{-1} were observed, corresponding to the υ(M─O) stretching vibration, and at 480 cm^{-1}, assigned to the υ(M─N) stretching vibration [19]. Overall, these results provide strong evidence of the successful synthesis of the oligomeric metal complex. The molecular weight analysis indicated the formation of four repeating units in the oligomer, with a number average molecular weight (Mn) of 2274 g/mole.

3.3 | Photophysical Properties

Figure 1 displays the absorption and fluorescence spectrum of the oligomeric metal complex **6** in a dilute DMSO solution. The absorption spectrum exhibits a broad and featureless band centered at 287 nm, corresponding to the characteristic absorption

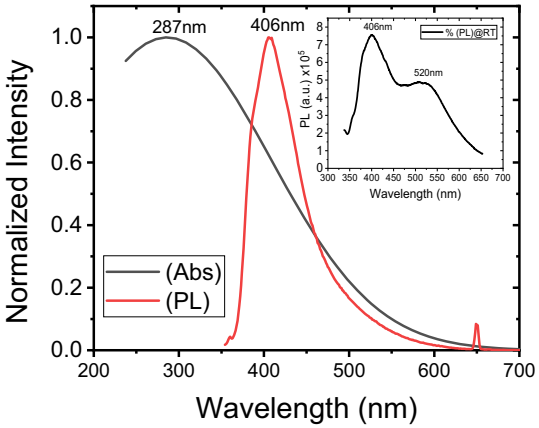

FIGURE 1 | Steady state normalized absorbance and fluorescence spectrum for oligomeric metal complex in a dilute DMSO 1 cm quartz cuvette. The excitation wavelength for PL measurement was 320 nm. Inset: Pulse spectra at 355 nm with 1 ns delay the fluorescence at 405 nm and (^{3}MLCT) metal-to-ligand charge transfer at 520 nm at room temperature can be observed.

peak of the 1,3,4-oxadiazole group, in line with previous findings within the range of 283–303 nm [24]. The absorption peak attributed to the 8-hydroxyquinoline metal complex [8HQ-Zn], typically observed at 300–400 nm, is concealed within this broad absorbance profile.

A steady-state fluorescence emission was detected at 406 nm, and it is proposed to originate from the 1,3,4-oxadiazole component [25]. Interestingly, the emission associated with ^{3}MLCT, possibly related to the 8-hydroxyquinoline metal complex, was not prominently displayed in the steady-state spectrum due to its relatively low intensity. Nevertheless, employing pulse laser excitation at 355 nm with a 1 ns delay allowed for partial reduction of the fluorescence emission intensity, facilitating the observation of both fluorescence at 406 nm and ^{3}MLCT emission at 520 nm, as depicted in the inset of Figure 1.

To conduct a comprehensive analysis of the PL emission of the oligomeric complex **6**, time-resolved analysis was performed at both room temperature and 14 K. The complex was blended with a PMMA film at a 1:100 weight ratio, and a casting film was applied to a quartz disc. Subsequently, the sample was cooled in a liquid helium cryostat and connected to a temperature controller. Three distinct spectral emissions were detected under various experimental configurations, as depicted in Figure 2a. At room temperature, a prominent prompt fluorescence originates from 1,3,4-oxadiazole monomer was observed at 406 nm, featuring an emission lifetime of 1.27 ns (Figure 3a). Under specific low-temperature conditions, a distinct emission with lower intensity was exclusively observed, peaking at 460 nm. This emission is attributed to the triple phosphorescence of the 1,3,4-oxadiazole group within complex **6** and exhibited a measured lifetime of 694 ms, as illustrated in Figure 3b. Additionally, a strong emission at 510 nm was evident, which could be ascribed to ^{3}MLCT originating from the 8HQ-Zn. This emission state exhibited a relatively short lifetime of 21 ns (Figure 3c). Notably, the short lifetime decay of this ^{3}MLCT emission indicates weak spin-orbital coupling, influenced by the Zn(II) metal with an atomic number of 30, below the threshold value of 40 required for strong singlet–triplet mixing [26]. The presence of these three

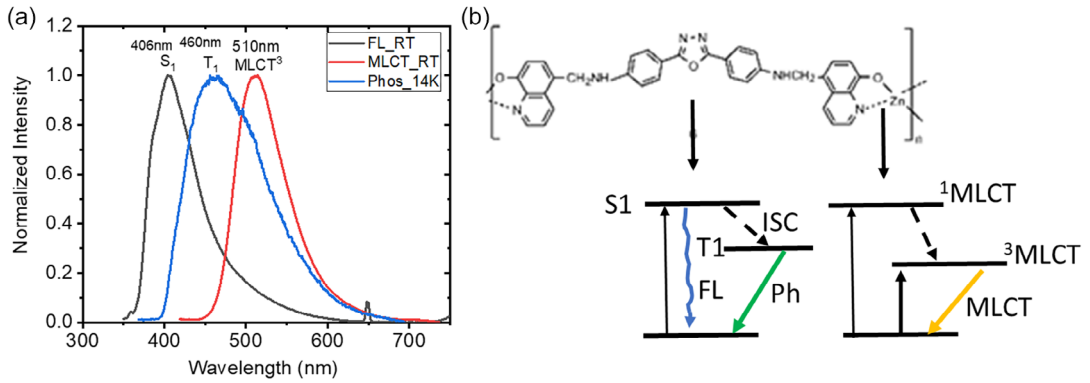

FIGURE 2 | (a) Room temperature prompt fluorescence and ^{3}MLCT and 14 K phosphorescence spectrum for **6** in PMMA 1:100 ww drop cast film. (b) The energy diagram for compound **6** illustrates the potential emission of three wavelengths originating from its dual electron-transport groups.

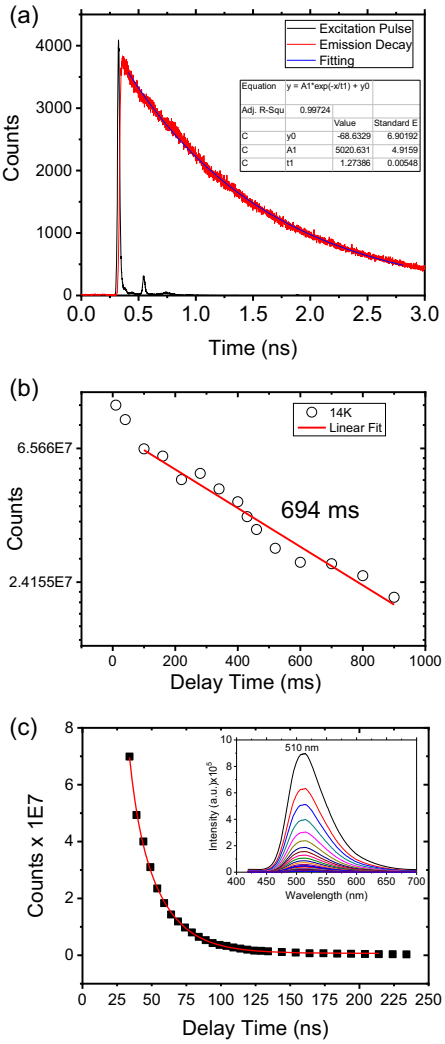

FIGURE 3 | Time-resolved analysis for **6** in a PMMA film: (a) Prompt fluorescence decay at room temperature, (b) phosphorescence decay at 14 K, and (c) metal-to-ligand charge transfer ^{3}MLCT decay at room temperature, inset the emission profile decay with increasing delay time. The excitation wavelength is 355 nm. The lifetimes are stated on the graphs. Figure 3a measured by direct decay of the emission at 406 nm. Figure 3b,c measured by emission profile delay time steps and integration times (gate) as described in the Supporting Information (Figures S3 and S4).

spectral emissions within a single compound **6** can be attributed to the hybrid monomer nature of the ligand, signifying a weak coupling between the 1,3,4-oxadiazole monomer and the 8HQ-Zn metal complex. These findings underscore the intriguing photophysical behavior of the oligomeric complex, thereby underscoring its potential significance in diverse applications.

3.4 | Electroluminance Properties

3.4.1 | OLED Device Characterization

The device structure of ITO/PEDOT:PSS (45 nm)/PVK (40 mg/mL): *x*% [6]: $Ir(ppy)_3$ (4% w/w)/LiF(1 nm)/Al(100 nm), where *x* varies from 5% to 40%, was explored, and it was found that **6** at 10% w/w provided the best device efficiency *T*. In comparison to similar devices utilizing PBD as an electron-transport material, the present oligomeric metal complex required only a 10% concentration to achieve best device performance [4]. Furthermore, since the concentration of compound **6** in the device is only 10%, it is hypothesized, that such a low loading does not adversely affect the device's operational stability through current-induced crystallization [14].

The device architecture is shown in Scheme 2a, while the energy levels of the materials used are illustrated in Scheme 2b. It's important to note that our efforts to measure the (HOMO–LUMO) highest occupied molecularorbitals - lowest unoccupied molecular orbitals levels of compound **6** were unsuccessful due to its poor solubility in the cyclic voltammetry electrolyte, which is attributed to its oligomeric nature. However, time-resolved analysis clearly indicates that the two electron-transport materials, PBD and 8-HQ-Zn, are linked within the oligomer chain without forming a new ground-state compound. Based on these time-resolved results, we infer that the HOMO–LUMO levels of compound **6** can be represented by two distinct HOMO–LUMO pairs, each corresponding to one of the electron-transport monomers, PBD and 8-HQ-Zn, as shown in Scheme 2b. The LUMO energy levels of PBD and 8-HQ-Zn are very similar (−2.4 and −2.3 eV, respectively) [27–29], suggesting that the new dual electron-transport oligomeric complex has a broader effective LUMO energy level. This broader LUMO facilitates efficient electron injection from the LiF/Al cathode, enabling the device to achieve peak efficiency at a lower electron-transport concentration (10% w/w) compared to using a single electron-transport

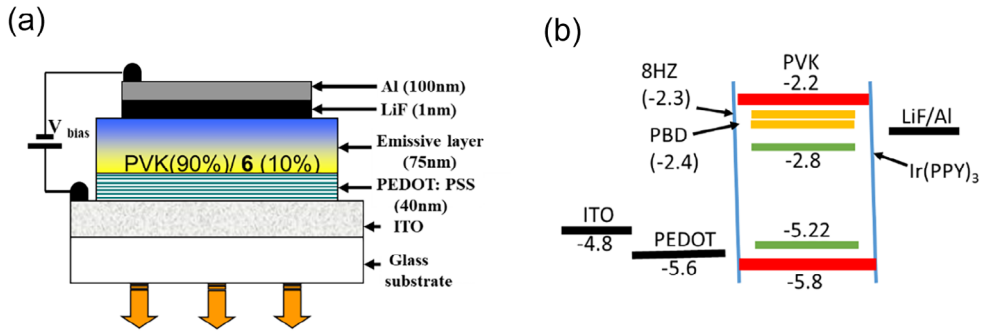

SCHEME 2 | The device architecture and energy levels for materials used in the device. All materials energy levels are in electronvolt (eV).

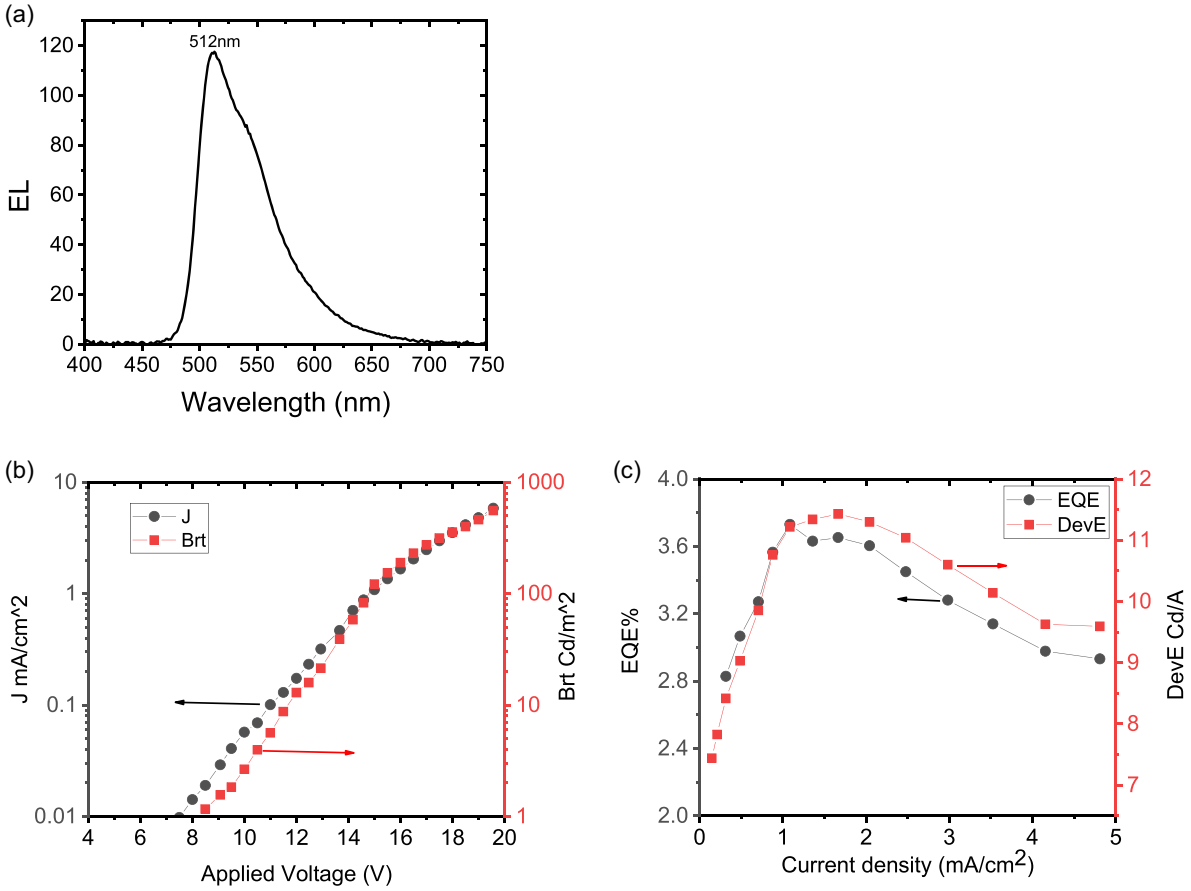

FIGURE 4 | (a) EL spectrum for devices with PVK as a host and **6** as EIT material, showing emission exclusively from $Ir(ppy)_3$ dopant. (b) *J*–*V* and *J*–brightness characteristics. (c) External quantum efficiency and device current efficiency.

material of (40% w/w). In Scheme 2b the HOMO energy levels of PBD and 8-HQ-Zn at (−6.2 and −6 eV respectively) were omitted for clarity.

Figure 4a illustrates the EL emission of the devices, predominantly originating from the dopant complex $Ir(ppy)_3$, with $\nu(0,0)$ transitions at 512 nm and a shoulder peak at 545 nm from $\nu(0,1)$ transitions [30]. The ^{3}MLCT emission of the metal oligomer at 510–520 nm overlaps with the $Ir(ppy)_3$ emission but has minimal impact on the device EL emission. The electrical characteristics of the device configuration, ITO/PEDOT:PSS (45 nm)/PVK:[**6**]:$Ir(ppy)_3$ (90 nm)/LiF (1 nm)/Al (100 nm), are shown in Figure 4b,c. The current density–voltage (*J*–*V*) and brightness–voltage (Br–V) are illustrated in Figure 4b, with a turn-on voltage at a brightness of 1 cd/m^2 measured at 8.2 V. Additionally, the device's external efficiency EQE% and current efficiency cd/A are shown in Figure 4c. The maximum EQE% and cd/A are measured at 3.6% and 11.5 cd/A, respectively. The moderate efficiency of the device and the relatively high turn-on voltage are likely attributed to the moderate solubility of **6**. Nevertheless, device optimization remains to be accomplished in the future stages of this study.

4 | Conclusion

In conclusion, a new EIT material in the form of a low-molecular-weight oligomer–metal complex has been successfully synthesized.

This metal electron-transport oligomer incorporates two electron-transport groups within a single compound, resulting in a hybrid ligand. The main advantages of this new hybrid oligomeric metal complex are to achieve the following points: (1) Oligomeric structure can be easily processed from solution (e.g., via spin-coating), offering a scalable and cost-effective alternative to vacuum deposition. (2) The oligomeric structure backbone serves as a scaffold that enables the incorporation of multiple electron-transport functionalities within a single material. (3) Covalent linkage of the two electron-transport moieties prevents phase segregation and ensures perfect stoichiometry.

Our research underscores the valuable insights that time-resolved analysis can provide into the chemical structure, enhancing our understanding alongside traditional chemical analyses. solubility of this compound is currently limited and requires improvement. Considering the two bioactive aspects of this oligomer, it holds promise as a potential bioactive material against various biological targets. The preliminary application of this oligomer as an electron-transport material in OLEDs has demonstrated were stable operation and moderate efficiency has been obtained at lower concentration compared to other electron-transport materials. Overall, this work represents a first attempt to the best of our knowledge in the field of electron-transport materials for OLEDs and offers potential applications in bioactive materials research. Further optimization and exploration of functional groups to improve solubility will be crucial for harnessing the full potential of this new oligomeric–metal complex in various applications.

Acknowledgments

The authors extend their heartfelt gratitude to the Iraqi Ministry of Higher Education and Scientific Research (MOHER) as well as the Physics Department at the University of Basrah for their invaluable support. This research received no external funding.

Conflicts of Interest

The authors declare no conflicts of interest.

Data Availability Statement

The data that support the findings of this study are available from the corresponding author upon reasonable request.

References

1. C. Adachi, T. Tsutsui, and S. Saito, "Organic Electroluminescent Device Having a Hole Conductor as an Emitting Layer," *Applied Physics Letters* 55, no. 15 (1989): 1489–1491.

2. R. Pode, "Organic Light Emitting Diode Devices: An Energy Efficient Solid State Lighting for Applications," *Renewable and Sustainable Energy Reviews* 133 (2020): 110043.

3. J.-S. Kim, R. H. Friend, I. Grizzi, et al., "Spin-cast Thin Semiconducting Polymer Interlayer for Improving Device Efficiency of Polymer Light-Emitting Diodes," *Applied Physics Letters* 87, no. 2 (2005): 023506.

4. H. A. Al Attar and A. P. Monkman, "Dopant Effect on the Charge Injection, Transport, and Device Efficiency of an Electrophosphorescent Polymeric Light-Emitting Device," *Advanced Functional Materials* 16, no. 17 (2006): 2231–2242.

5. D. Chen, W.-Z. He, H.-S. Liao, et al., "Benzimidazole/Carbazole-based Bipolar Host Materials for Highly Efficient Green Phosphorescent OLEDs with Negligible Efficiency Roll-off," *Organic Electronics* 113 (2023): 106715.

6. J. W. Park, J. Y. Oh, H. S. Hwang, et al., "Energy Barrier Reduction and Exciton Confinement Using an Intermediate Blocking Layer in Organic Light-emitting Diodes," *Japanese Journal of Applied Physics* 49, no. 11R (2010): 110204.

7. H. A. Al-Attar, G. C. Griffiths, T. N. Moore, et al., "Highly Efficient, Solution-Processed, Single-Layer, Electrophosphorescent Diodes and the Effect of Molecular Dipole Moment," *Advanced Functional Materials* 21, no. 12 (2011): 2376–2382.

8. C. Adachi, T. Tsutsui, and S. Saito, "Blue Light-Emitting Organic Electroluminescent Devices," *Applied Physics Letters* 56, no. 9 (1990): 799–801.

9. Y. Cao, I. D. Parker, G. Yu, et al., "Improved Quantum Efficiency for Electroluminescence in Semiconducting Polymers," *Nature* 397, no. 6718 (1999): 414–417.

10. B. Pashaei, S. Karimi, H. Shahroosvand, et al., "Polypyridyl Ligands as a Versatile Platform for Solid-state Light-emitting Devices," *Chemical Society Reviews* 48, no. 19 (2019): 5033–5139.

11. J.-W. Liu, H.-C. Zhou, Z.-K. Wang, et al., "Distinct Ir(III) Complexes Containing Unsymmetric Ligands with Fluorene-oxadiazole Groups and Their Performance of Organic Light-emitting Diodes," *Dyes and Pigments* 202 (2022): 110252.

12. Y. Tan, Z. Wang, C. Wei, et al., "Nondoped Deep-blue Fluorescent Organic Electroluminescent Device with CIEy = 0.06 and Low Efficiency Roll-off Based on Carbazole/Oxadiazole Derivatives," *Organic Electronics* 69 (2019): 77–84.

13. H. Al-Attar, A. A. Alwattar, A. Haddad, et al., "Polylactide-perylene Derivative for Blue Biodegradable Organic Light-emitting Diodes," *Polymer International* 70, no. 1 (2021): 51–58.

14. B. Schulz, M. Bruma, and L. Brehmer, "Aromatic Poly (1, 3, 4-Oxadiazoe) s as Advanced Materials," *Advanced Materials* 9, no. 8 (1997): 601–613.

15. C. Chen and J. Shi, "Metal Chelates as Emitting Materials for Organic Electroluminescence," *Coordination Chemistry Reviews* 171 (1998): 161–174.

16. C. Wu, J. Chun, P. Burrows, et al., "Poly (p-phenylene Vinylene)/Tris (8-hydroxy) Quinoline Aluminum Heterostructure Light Emitting Diode," *Applied Physics Letters* 66, no. 6 (1995): 653–655.

17. D. L. Thomsen, T. Phely-Bobin, and F. Papadimitrakopoulos, "Zinc-Bisquinoline Coordination Assemblies of High Refractive Index and Film Uniformity," *Journal of the American Chemical Society* 120, no. 24 (1998): 6177–6178.

18. C. Schmitz, H.-W. Schmidt, and M. Thelakkat, "Lithium– Quinolate Complexes as Emitter and Interface Materials in Organic Light-emitting Diodes," *Chemistry of Materials* 12, no. 10 (2000): 3012–3019.

19. Y. He, C. Zhong, A. He, et al., "Synthesis and Luminescent Properties of Novel Bisfunctional Polymeric Complexes Based on Carbazole and 8-hydroxyquinoline Groups," *Materials Chemistry and Physics* 114, no. 1 (2009): 261–266.

20. W. Gurnule, K. Vajpai, R. Mankar, et al., "Photoluminescence Studies of Copolymer Metal Complexes with 8-hydroxyquinoline, Hexamethylenediamine and Formaldehyde," *Materials Today: Proceedings* 29 (2020): 974–980.

21. V. Prachayasittikul, S. Prachayasittikul, S. Ruchirawat, et al., "8-Hydroxyquinolines: A Review of Their Metal Chelating Properties and Medicinal Applications," *Drug Design, Development and Therapy* (2013): 1157–1178.

22. I. M. D. Loredana Vacareanu and M. Grigoras, "Polyimines with Electron-Donating and Accepting Groups: Synthesis and Characterization," *Revista de Chimie* 61, no. 1 (2010): 4.

23. L. Feng, X. Wang, and Z. Chen, "Synthesis and Photophysics of Novel 8-hydroxyquinoline Aluminum Metal Complex with 1, 3, 4-oxadiazole Units," *Spectrochimica Acta Part A: Molecular and Biomolecular Spectroscopy* 71, no. 2 (2008): 312–316.

24. J. B. Lambert, L. Verbit, R. G. Cooks, and H. G. Stout, *Organic Structural Analysis* 13 (1976): 596.

25. M. Homocianu and A. Airinei, "1, 3, 4-Oxadiazole derivatives. Optical properties in Pure and Mixed Solvents," *Journal of Fluorescence* 26 (2016): 1617–1635.

26. Q.-D. Liu, R. Wang, and S. Wang, "Blue Phosphorescent Zn(ii) and Orange Phosphorescent Pt(ii) Complexes of 4,4′-diphenyl-6,6′-dimethyl-2,2′-bipyrimidine," *Dalton Transactions* 14 (2004): 2073–2079.

27. H. A. Al-Attar and A. P. Monkman, "Solution Processed Multilayer Polymer Light-emitting Diodes Based on Different Molecular Weight Host," *Journal of Applied Physics* 109, no. 7 (2011): 074516.

28. J.-C. Chen, C.-J. Chiang, and Y.-C. Liu, "Synthesis, Optical and Electrochemical Properties of Novel Hole-blocking Poly(biphenylene-1,3,4-oxadiazole) Containing Electron-withdrawing Trifluoromethyl Groups," *Synthetic Metals* 160, no. 17 (2010): 1953–1961.

29. H. Nishikiori, S. Nakamura, D. Natori, et al., "Potential Levels of Metal Complexes of 8-hydroxyquinoline," *Chemical Physics Letters* 662 (2016): 146–151.

30. C. Soldano, O. Laouadi, and K. Gallegos-Rosas, "TCTA: Ir(ppy)3 Green Emissive Blends in Organic Light-Emitting Transistors (OLETs," *ACS Omega* 7, no. 48 (2022): 43719–43728.

Supporting Information

Additional supporting information can be found online in the Supporting Information section. Supplementary information may be found in the online version of this article. **Supporting Fig. S1:** 1H NMR spectra of the new ligand **5**. **Supporting Fig. S2:** FT-IR spectra of the new oligomeric metal complexes **6**. **Supporting Fig. S3:** Phosphorescence emission profile decay for 6 at 14 K with delay steps increment of 60 ms and integration time (gate) of 30 ms. **Supporting Fig. S4:** ^{3}MLCTemission profile decay for **6** at room temperature with delay steps increment of 5 ns and integration time (gate) of 5 ns. **Supporting Fig. S5:** PL emission for **6** at different solvent showing excimer formation when the solvent Toluene due to weak solubility.